IJE TRANSACTIONS C: Aspects Vol. 27, No. 3, (March 2014) 441-448

International Journal of Engineering

Journal Homepage: www.ije.ir

A Study on Combination of von Mises and Tresca Yield Loci in Non-associated Viscoplasticity

F. Moayyedian *, M. Kadkhodayan

Department of Mechanical Engineering, Ferdowsi University of Mashhad, Mashhad, Iran

PAPER INFO

Paper history:
Received 08 April 2013
Received in revised form 10 July 2013
Accepted 22 August 2013

Keywords:
Viscoplastic
Thick Walled Cylinder
Time Stepping Scheme
Internally Pressurized

ABSTRACT

In this study, a non-associated viscoplastic flow rule (NAVFR) with combining von Mises and Tresca loci in place of yield and plastic potential functions and vice verse is presented. It is shown that the proposed NAVFR can be adopted to forecast the experimental events more accurate than the conventional associated viscoplastic flow rules (AVFR). This outcome obtained with the aid of fully implicit time stepping scheme and discussing the other studies on plastic potential flow rules and also experimental results.

doi: *10.5829/idosi.ije.2014.27.03c.12*

NOMENCLATURE

B	The nodal strain-displacement matrix
d	The nodal displacement
$\hat{D}$	The consistent elastic-plastic modulus
E	Young modulus
f	The external work
F	The yield locus
F_0	The uniaxial yield stress
G	The plastic potential locus
H'	Plastic modulus
J_1	The first invariant of stress
J_2', J_3'	The second and the third invariants of deviatoric stress
M, N	Arbitrary prescribed constants
t	Time
V	The pseudo load

Greek Symbols

γ	The fluidity parameter
Γ	The Lode parameter
ε	Strain
ε_{vp}	Viscoplastic strain
$\dot{\varepsilon}_{vp}$	Viscoplastic strain rate
θ	The angle of loading in deviator plane
Θ	Time stepping parameter
κ	The hardening parameter
ν	Poisson ratio
σ	Stress
Ψ	The residual forces
Φ	Positive monotonic increasing function

1. INTRODUCTION

Time rate effects are always present to some degree in all inelastic deformations (time dependant mechanical behaviors). Metals especially under high temperatures show signs of simultaneously the phenomena of creep (viscoelasicity) and viscoplasticity. The former is essentially a redistribution of stress and/or strains with time under elastic material response while the latter is a time dependant plastic deformation. In this research, a NVFR rule is studied and introduced to provide a new approach to problems of time dependant and independent plasticity. Providing solutions to time-

*Corresponding Author Email: farzad_moayyedian@yahoo.com (F. Moayyedian)

dependent elastic-plastic problems can provide effective solutions for classical elastic-plastic situations. It can be shown that the steady-state solution of the viscoplastic problems is identical to its corresponding conventional static elastic-plastic one. In the following, the studies of the previous researchers on the mentioned issue are reviewed.

A non-associated flow rule based on a pressure sensitive yield locus with isotropic hardening was proposed by Stoughton and Yoon [1]. The significance of their work was that their model distorted the shape of the yield function in tension and compression, fully accounting for the strength differential effect (SDE). A return mapping algorithm for cyclic viscoplastic constitutive models that included material memory effects was presented by Kumar and Nukala [2]. Their constitutive model was based on multi-component forms of kinematic and isotropic hardening variables in conjunction with von Mises yield locus. Armstrong-Fredreick type rules [3] were used to describe the non-linear evolution of each of the multi-component kinematic hardening variables. A design sensitivity analysis approach by the consistent tangent operator concept-based boundary element implicit algorithm was presented by Liang et al. [4]. It was included geometry, elasto-visco-plastic material and boundary condition parameters. A finite element formulation based on non-associated plasticity was developed by Cvitanic et al. [5]. The yield and plastic potential functions were considered as two different functions with functional form. With use of five different material data for aluminum and stainless steel alloys, five material models ranging in complexity from a von Mises model based on isotopic hardening to a non-associated flow rule model based on anisotropic hardening was calibrated and evaluated by Stoughton and Yoon [6]. Their model was expected to lead to a significant improvement in stress prediction under conditions dominated by proportional loading. It also expected to improve the accuracy of springback, tearing and earning predictions for these processes. Using experimental and numerical studies, Gao et al. [7] showed that the stress state had strong effects on both plastic response and ductile fracture behavior of an aluminum 5083 alloy. As a result, the hydrostatic stress and the third invariant of the stress deviator (which was related to the Lode angle) needed to be incorporated in material modeling. Mohr et al. [8] applied a combined normal and tangential loads to a flat specimen in order to characterize the sheet metal response under 20 distinct multi-axial loading states. The comparison of the experimental results with the plasticity model predictions revealed that both associated and non-associated quadratic formulations provided good estimates of the stress-strain response under multi-axial loading. However, the non-associated model was recommended when an accurate description of the thinning behavior was important. A consistent tangent stiffness was introduced by Romano et al. [9] to improve the asymptotic convergence rate of the iterative correction algorithm for the evaluative analysis of elastoplastic structures. An estimation of the tangent stiffness associated with finite step elastoplastic and elastoviscoplastic constitutive models was given. A generalized finite element formulation of stress integration method was developed by Taherizadeh et al. [10]. It was for non-quadratic yield functions and potentials with mixed non-linear hardening under non-associated flow rule. Different approaches to analyze the anisotropic behavior of sheet materials were compared. The first model was based on a non-associated formulation with both quadratic yield and potential functions in the form of Hill's and the second one was an associated non-quadratic model Yld2000-2d. The third model was a non-quadratic non-associated model in which the yield function was defined based on Yld91 and the potential function was defined based on Yld89. A plasticity model for isotropic materials, which was a function of the hydrostatic stress as well as the second and third invariants of the stress deviator with special attention to adopt the non-associated flow rule was described by Gao et al. [11]. It was implemented in finite element method including integration of the constitutive equations using the backward Euler method and formulation of the consistent tangent modulus. A thermodynamic consistent, small-strain, non-unified model to capture the irregular rate dependency included in the strain controlled inelastic responses of polymers at the glassy state was developed by Voyiadjis et al. [12]. The model was considered as a generalized Frederick-Armstrong-Philips-Chaboche (FAPC) [13]. A consistent formulation of the non-associated plasticity for soil was proposed by Berga [14]. He presented the implicit standard material method and a methodology to build a full model for the boundary value problem. Moayyedian and Kadkhodayan [15] studied the derivation of the second differentiation of a general yield surface by implicit time stepping method along with its consistent elastic-plastic modulus. Moreover, the explicit, trapezoidal implicit and fully implicit time stepping schemes were compared in rate-dependant plasticity. Finally, it was shown that implementing fully implicit time stepping scheme in rate-dependant plasticity predicts experimental results more accurate than the other schemes.

The main goal of this study is arisen from combining of von Mises and Tresca loci as the yield and plastic potential functions. To show the ability of the proposed NAVFR, the global finite element code of a two-dimensional problem with the aid of references [16-20] in finite element and [21-25] in plasticity theories is developed. An internally elastic-viscoplastic pressurized thick walled cylinder is considered with perfectly plastic and linear-isotropic hardening behaviour of material and coded in Compaq Visual Fortran Professional Edition

6.5.0. It should be noted that to employ the implicit time stepping scheme viscoplasicty, the first and the second differentiation of a yield or plastic potential locus should be available. A general derivation required for the latter subject is used from the previous work of authors [15].

2. GENERAL INTERPRETATIONS

The general form of a yield locus of an isotropic material is $F(J_1,J_2^{'},J_3^{'})$ which J_1 is the first stress invariant and $J_2^{'}$ and $J_3^{'}$ are the second and the third invariants of deviatoric stresses. J_1 shows the dependency of the yield locus to the hydrostatic pressure while $J_2^{'}$ and $J_3^{'}$ show the dependency of the yield locus to deviatoric stresses. Another parameter which can help to interpret the state of stress in deviatoric plane is the angle of loading in deviatoric plane, θ, see Figure 1. This parameter can be defined as following [15]:

$$\sin 3\theta = -\frac{3\sqrt{3}}{2}\frac{J_3'}{(J_2')^{\frac{3}{2}}}. \quad (1)$$

For an isotropic material, it would be sufficient if the yield locus is studied in the region of $-\frac{\pi}{6} \le \theta \le +\frac{\pi}{6}$. Hence, the Lode parameter can be defined as $\Gamma = -\sqrt{3}\,tan\,\theta$. Therefore, the yield locus can be mentioned in $-1 \le \Gamma \le +1$. It can be demonstrated that for pure shear, $\Gamma = \theta = 0$, for pure tension, $\theta = -\frac{\pi}{6}$, $\Gamma = +1$ and for pure compression, $\theta = +\frac{\pi}{6}$, $\Gamma = -1$. The presentation of von Mises and Tresca yield loci which is proper for the computational purposes is observed in Table 1. Where σ_Y is the uniaxial yield stress, κ is the hardening parameter [15]. Figure 1 shows the presentation of the von Mises and Tresca loci in deviatoric plane.

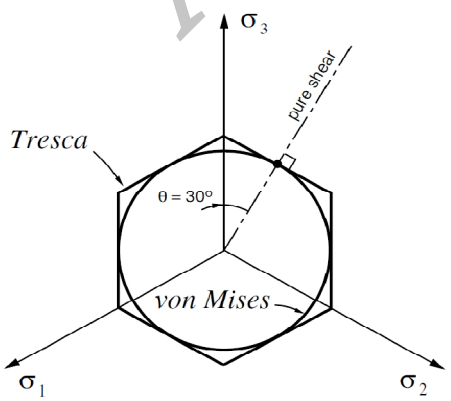

Figure 1. Presentation of von Mises and Tresca loci in π plane [17].

TABLE 1. Two classic yield loci [15]

von Mises	Tresca
$\sqrt{3}(J_2^{'})^{\frac{1}{2}} = \sigma_Y(\kappa)$	$2(J_2^{'})^{\frac{1}{2}} cos\,\theta = \sigma_Y(\kappa)$

3. NON-ASSOCIATED VISCOPLASTIC FLOW RULE (NAVFR)

The onset of viscoplastic behavior is governed by a scalar yield condition of the form:

$$F(\sigma, \varepsilon_{vp}) - F_0 = 0, \quad (2)$$

In which, F_0 is the uniaxial yield stress which may be a function of a hardening parameter κ. It is assumed that viscoplastic flow only occurs for values of $F > F_0$ [15]. A common explicit form of viscoplastic strain rate is offered by the following viscoplastic flow rule:

$$\{\dot{\varepsilon}_{vp}^n\} = \gamma < \Phi(F) > \left\{\frac{\partial G}{\partial \sigma}\right\}, \quad (3)$$

where, $G = G(\sigma, \varepsilon_{vp}, \kappa)$ is a plastic potential locus and γ is a fluidity parameter controlling the plastic flow rate. The term $\Phi(F)$ is a positive monotonic increasing function for $x > 0$ and the notation $\langle\ \ \rangle$ implies:

$$\begin{cases} < \Phi(x) > = \Phi(x) & x > 0, \\ < \Phi(x) > = 0 & x \le 0. \end{cases} \quad (4)$$

For the associated plasticity situations, $G \equiv F$. Different functions for Φ have also been recommended as following [15]:

$$\begin{cases} \Phi(F) = e^{M\left(\frac{F-F_0}{F_0}\right)} - 1, \\ \Phi(F) = \left(\frac{F-F_0}{F_0}\right)^N. \end{cases} \quad (5)$$

M and N are arbitrary prescribed constants.

In the following, the symbol $\{\ \ \}$ is used for a 6×1 vector and the symbol $[\ \ ]$ for a 6×6 matrix in three dimensional stress space.

3. 1. The Viscoplastic Strain Increment With the strain rate law which is expressed by Equation (3), a strain increment $\{\Delta\varepsilon_{vp}\}^n$ occurring in a time interval $\Delta t_n = t_{n+1} - t_n$ using a time stepping scheme was defined as [15]:

$$\{\Delta\varepsilon_{vp}\}^n = \Delta t_n \left((1-\Theta)\{\dot{\varepsilon}_{vp}\}^n + \Theta\{\dot{\varepsilon}_{vp}\}^{n+1}\right). \quad (6)$$

For $\Theta = 0$ the Euler time integration scheme is obtained which is also referred to 'fully explicit' (or forward difference method) since the strain increment is completely determined from the existing conditions at time t_n. On the other hand, taking $\Theta = 1$ gives a 'fully implicit' (or backward difference) scheme with strain increment being determined from the strain rate corresponding to the end of the time interval. The case

$\Theta = \frac{1}{2}$ results in the so-called 'implicit trapezodial' scheme which is also known generally as the Crank-Nicolson rule [15].

To define $\{\dot{\varepsilon}_{vp}^{n+1}\}$ in Equation (6), the limited Taylor series expansion can be used [15]:

$$\{\dot{\varepsilon}_{vp}\}^{n+1} = \{\dot{\varepsilon}_{vp}\}^{n} + [H]^{n}\{\Delta\sigma^{n}\}, \quad (7)$$

where,

$$[H]^{n} = \left[\frac{\partial \dot{\varepsilon}_{vp}^{n}}{\partial \sigma}\right], \quad (8)$$

and $\overrightarrow{\Delta\sigma^{n}}$ is the stress change occurring in the time interval $\Delta t_n = t_{n+1} - t_n$. Thus, Equation (6) can be written as:

$$\{\Delta\varepsilon_{vp}\}^{n} = \{\dot{\varepsilon}_{vp}\}^{n}\Delta t_n + [C]^{n}\{\Delta\sigma^{n}\}, \quad (9)$$

where,

$$[C]^{n} = \Theta\Delta t_n [H]^{n}. \quad (10)$$

3. 2. Evaluation of $\overrightarrow{H^n}$ using NAVFR To employ the fully implicit or semi-implicit (trapezoidal) time stepping scheme, the matrix $[C]^n$ is required. It can be expressed in terms of $[H]^n$ as indicated in Equation (8). Matrix $[H]^n$ has to be explicitly determined from the plastic potential locus assumed for material behavior. From Equations (3) and (9), it is found:

$$\vec{H} = \gamma\Phi\left[\frac{\partial^2 G}{\partial\sigma^2}\right] + \gamma\frac{d\Phi}{dF}\left(\left\{\frac{\partial G}{\partial\sigma}\right\}\left\{\frac{\partial G}{\partial\sigma}\right\}^{T}\right). \quad (11)$$

The symbol $\langle\ \ \rangle$ on Φ and the superscript n are dropped for convenience. The approach of calculating $\left\{\frac{\partial G}{\partial\sigma}\right\}$ and $\left[\frac{\partial^2 G}{\partial\sigma^2}\right]$ for a general yield or plastic potential locus is presented in previous work of the authors [15].

3. 3. Solution Sequence for Stress updating using (NAVFR) The essential steps in solving process are summarized here. The solution begins from a known initial conditions at $t = 0$, which are the static elastic situation. At this stage, d^0, F^0, G^0, ε^0 and σ^0 are known and $\varepsilon_{vp}^0 = 0$. The time marching scheme described in the previous section; then it is employed to advance the solution.

4. RESULTS AND DISCUSIONS

In this section, with considering the mechanical properties, Young modulus of elasticity, $E = 21000\ \frac{dN}{mm^2}$, Poisson ratio, $\nu = 0.3$, yield stress, $F_0 = \sigma_Y = 24.0\ \frac{dN}{mm^2}$, plastic modulus, $H' = 0.0\ \frac{dN}{mm^2}$ for perfect plastic and $H' = \frac{E}{10}$ for isotropic linear hardening behaviour of materials, fluidity parameter, $\gamma = 0.001/day$, inner radius of the cylinder, $a = 100\ mm$ and outer radius of the cylinder, $b = 200\ mm$, and the flow function $\Phi(F) = F$ and employing the fully implicit time stepping scheme $(\Theta = 1)$, von Mises and Tresca loci are combined by considering them in the role of yield and plastic potential functions and vice verse. The abbreviations of (V) and (T) stand for the von Mises and Tresca loci, respectively. Moreover, in symbol of (□-□), the first and second letters show the yielding and plastic potential functions used in the analysis, respectively. To compare the latter effects on the obtained results the steady state condition at 100% over strain can be observed in Figure (2) for an elastic-viscoplastic internally pressurised vessel. The results show that employing NAVFR (V-T) which is comparing with AVFR (V-V) and also NAVFR (T-V) which is comparing with AVFR (T-T) predict the experimental results more accurately. It is seen that (V-V) overestimates and (T-T) underestimates the experimental data. Moreover, it can be observed that for the less ratios of $\frac{b}{a}$, using Tresca locus along with the AVFR (T-T) cause better accuracy than that of the von Mises AFVR.

Consequently, it can be found out that using NAFVR may predict the experimental results more precisely. For instance, for $\frac{b}{a} \leq 2$ and $\frac{b}{a} \geq 2$ using (T-V) and (V-T) could provide better accuracy, respectively.

Figures (3, 4) demonstrate the variation of circumferential strain at the outer surfaces $\frac{b}{a} = 1{,}6$ and $\frac{b}{a} = 2.4$ (the most accurate ratio of $\frac{b}{a}$ with employing (T-T) and (V-T) as it seen in Figure (2)) with time and also the steady state circumferential stress distributions in $1 \leq \frac{r}{a} \leq 1.6$ and $1 \leq \frac{r}{a} \leq 2.4$ for perfect-plastic materilas with considering AVFR and NAVFR. Figures (5, 6) show the previous items with considering isotropic linear hardening behavior of materials.

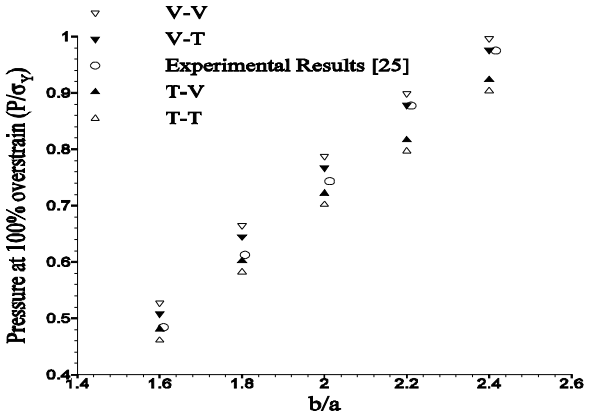

Figure 2. Comparison between the experimental results and $V-V$, $V-T$, $T-V$ and $T-T$ in steady state condition.

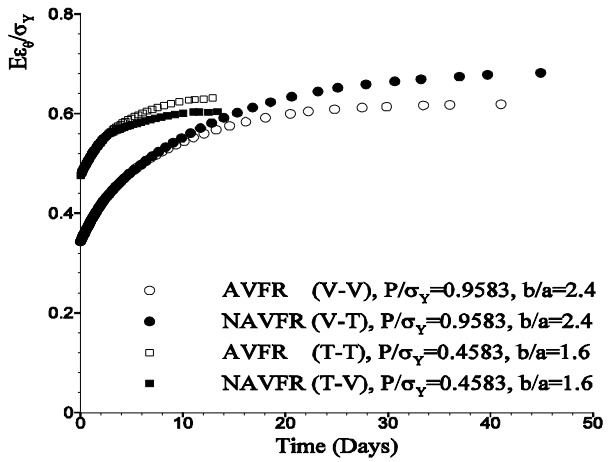

Figure 3. Comparison between the $V-T$ and $V-V$ and also $T-T$ and $T-V$ for variation of circumferential strain at the outer surface with time and perfect plastic behavior of materials.

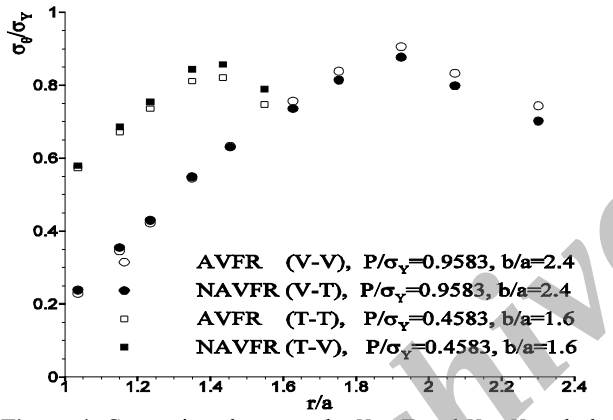

Figure 4. Comparison between the $V-T$ and $V-V$ and also $T-T$ and $T-V$ for variation of circumferential stress with radial distance and perfect plastic behavior of materials.

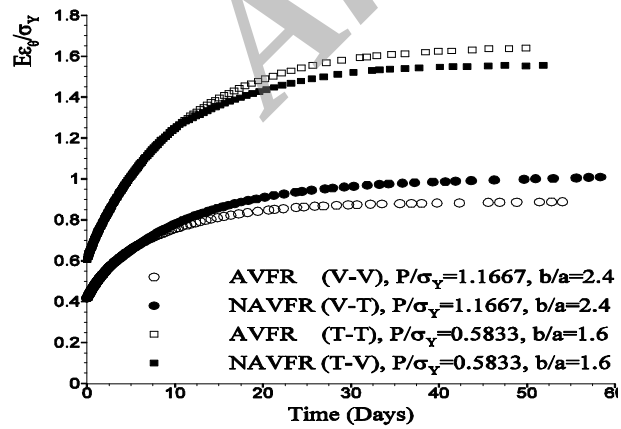

Figure 5. Comparison between the $V-T$ and $V-V$ and also $T-T$ and $T-V$ for variation of circumferential strain at the outer surface with time with considering linear isotropic hardening behavior of materials.

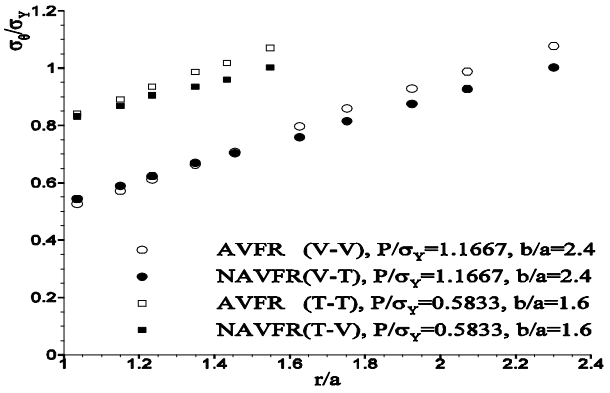

Figure 6. Comparison between the $V-T$ and $V-V$ and also $T-T$ and $T-V$ for variation of circumferential stress with radial distance and with considering linear isotropic hardening behavior of materials.

Figures (3, 5) show that the strains predicted by NAFVR, V-T (T-V) are less than that of AFVR, V-V (T-T) for the same time for $\frac{b}{a}=2.4$ ($\frac{b}{a}=1{,}6$). Moreover, Figures (4, 6) show that the steady state stresses predicted by NAFVR, T-V are more than those of AFVR, T-T in the interval of $1\leq\frac{r}{a}\leq 1.6$ and for $\frac{r}{a}<1.4$ ($\frac{r}{a}\geq 1.4$) the hoop stresses predicted by NAVFR V-T are less than AVFR V-V.

Finally, by considering Figures (3-6), it can be found that with increasing the load and hardening, the differences between AFVR and NAFVR increase.

To investigate the proposed NAVFR more precisely, the subsequent investigations can be helpful. From Table 1, the Tresca yield locus can be written as below:

$$2(J_2')^{\frac{1}{2}}\cos\theta-\sigma_Y=0,-\frac{\pi}{6}\leq\theta\leq\frac{\pi}{6}, \tag{12}$$

or,

$$J_2'\cos^2\theta=\frac{\sigma_Y^2}{4}. \tag{13}$$

Using Equation (1), it can be found that:

$$\mathrm{Cos}^2\,\theta=1-\alpha\frac{J_3'^{\,2}}{J_2'^{\,3}}, \tag{14}$$

where,

$$\begin{cases}\alpha=\frac{27}{4}\beta,\\ \beta=\frac{\sin^2\theta}{\sin^2 3\theta}.\end{cases} \tag{15}$$

Consequently, the Tresca locus can be shown as following:

$$J_2'\left(1-\alpha\frac{J_3'^{\,2}}{J_2'^{\,3}}\right)=\frac{\sigma_Y^2}{4}. \tag{16}$$

Using Equation (15) and the range of θ in Equation (12), the range of α can be determined as $\frac{3}{4}\leq\alpha\leq\frac{27}{16}$ or $0.75\leq\alpha\leq 1.6875$. Moreover, some experimental

studies show that the plastic potential locus can be as following [21]:

$$G(J_2',J_3') = J_2'\left(1 - 0.73\frac{J_3'^{\,2}}{J_2'^{\,3}}\right), \quad (17)$$

It can predict the behavior of material more accurately than AVFR, V-V. Comparison Equation (16) with Equation (17) shows that the new plastic potential locus is nearly equal to Tresca locus in pure shear. Furthermore, the direction of normal to the Tresca locus is constant in the range of $-\frac{\pi}{6} \le \theta \le \frac{\pi}{6}$. Hence, considering (V-T) can predict the experimental results more accurately compared to (V-V). In addition, Gao, et al. [11] used yield and plastic potential loci as below:

$$\begin{cases} F = \left(c_1 J_1^6 + 27J_2'^{\,3} + b_1 J_3'^{\,2}\right)^{\frac{1}{6}}, \\ G = \left(c_2 J_1^6 + 27J_2'^{\,3} + b_2 J_3'^{\,2}\right)^{\frac{1}{6}}, \end{cases} \quad (18)$$

where,

$$\begin{cases} c_1 = \left(a_1 + \frac{4}{729}b_1 + 1\right)^{-\frac{1}{6}}, \\ c_2 = \left(a_2 + \frac{4}{729}b_2 + 1\right)^{-\frac{1}{6}}. \end{cases} \quad (19)$$

Comparing the model with different experimental results, they concluded that selecting $a_1 = a_2 = 0$ and $b_1 = -60.75$ and $b_2 = -25$ could predict the experimental data with good accuracy. It can be deduced that they nearly used T-V in their numerical calculations and showed that it is more accurate than AVFR, V-V.

From previous sections, it is realized that increasing the load step and considering hardening material increase the difference between NAVFR and AVFR. Moreover, another main reason for this difference can be attributed to the combination of loading (tention-shear). To investigate this issue, the Lode parameter, Γ, is considered. Figures (7, 8) show the variation of Lode parameter (in outer surface of the vessel) with time and angle α when AVFR based on both von Mises and Tresca yielding loci is used, respectively. As it is apparent, in pure shear the orthogonal vectors to Tresca and von Mises surfaces have the same directions (not the same values). Now, when the loading is such that $\Gamma \longrightarrow 0$, then the difference between the directions of the vectors of plastic strain increment for von Mises and Tresca decreases. On the other hand, when the loading is such that $\Gamma \longrightarrow \pm 1$, the difference increases. In other words, as the loading condition varies in such a way that $\Gamma \longrightarrow \pm 1$, the difference between the AFVR and NAVFR becomes higher. Figure (9) shows that the maximum difference between the AVFR and NAVFR happens in the outer surface of the vessel and for the current loading condition, the Load parameter is $\Gamma \cong -0.4$ in the outer surface. The difference between the results obtained by considering perfect-plastic behavior of matrials in Figures (3, 4) is solely because of the combination of loading. However, these differences become higher when in addition to combination of loading the isotropic hardening is also considered (see Figures (5, 6)). Therefore, for the problems with non-linear isotropic hardening in conjunction with the load condition in deviatory plane as $\Gamma \longrightarrow \pm 1$, the difference between the presented NAVFR and the corresponding AVFR becomes maximum. Figure (10) shows the variation of steady Lode parameter with different ratios of $\frac{b}{a}$ at 100% over strain. It is evident that for both (V-V) and (T-T), there is almost no change for Lode parameter in outer surface of the vessel. Therefore, it can be expected that the differences between the NAFVR and AFVR, i.e. between (V-V) and (V-T) and also (T-T) and (T-V), have to remain constant approximately for different ratios of $\frac{b}{a}$ as it can be observed in Figure (2).

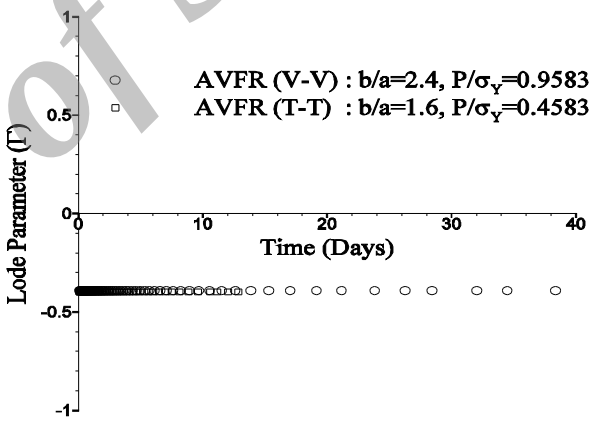

Figure 7. Variation of Lode parameter at outer surface versus time with perfect-plastic material.

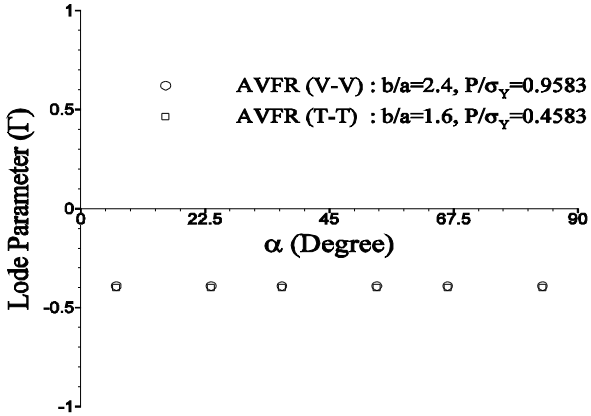

Figure 8. Variation of steady state Lode parameter versus angle α with perfect-plastic material.

It was expected in AVFR (V-V) or (T-T) when $\Gamma \to \pm 1$ the difference between NAVFR (V-T) or (T-V) becomes more obvious. In Figure 14, with AVFR, V-V (T-T), when $\frac{r}{a} = 2.4$ ($\frac{r}{a} = 1.6$), $\Gamma \cong -0.4$. Therefore, it was expected in outer face of the vessel, the difference between V-V (T-T) and V-T (T-V) becomes maximum. In Figures (4, 6), this maximum difference in outer face of the vessel can be observed.

In Figure (9), for AVFR, V-V when $\frac{r}{a} = 1.41341$, the Lode parameter becomes zero ($\Gamma = 0$), when $1 \leq \frac{r}{a} < 1.41341$, sign of the Lode parameter becomes positive ($\Gamma > 0$) and when $1.41341 < \frac{r}{a} \leq 2.4$, it becomes negative ($\Gamma < 0$). The effect of changing the Load parameter can be observed in Figures (4, 6) with employing NAVFR (V-T). In Figure (9), for AVFR, T-T when $1 \leq \frac{r}{a} \leq 2.4$, sign of the Lode parameters remains negative ($\Gamma < 0$). Therefore, sign of Lode parameter is unchanged unlike V-V and this effect can be seen in Figures (4, 6) when NAVFR (T-V) is employed. Finally, it can be realized that the difference between AVFR and NAVFR has a direct effect on the sign and value of the Lode parameter.

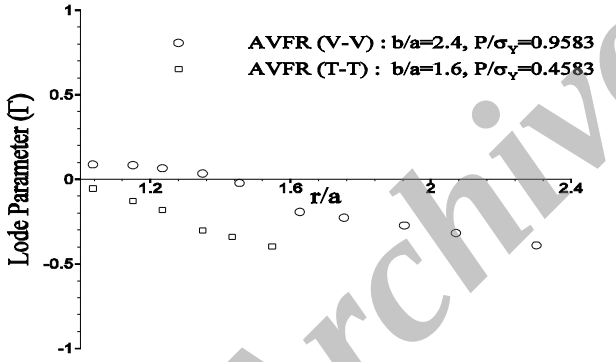

Figure 9. Variation of steady state Lode parameter versus radius with perfect-plastic material and von Mises and Tresca criteria.

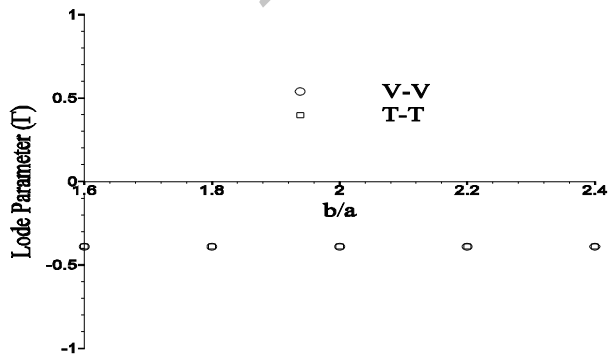

Figure 10. The variation of steady state Lode parameter with $\frac{b}{a}$ at 100% over strain.

5. CONCLUSIONS

The main idea in this research is arisen from combining von Mises and Tresca loci for the yield and plastic potential functions and vice verse. During this investigation, the experimental observation and analysis of plastic potential locus is discussed and the following results are obtained:

1- The case of (V-V) overestimates and (T-T) underestimates the experimental data.
2- Employing NAVFR (V-T) compared with AVFR (V-V) and also NAVFR (T-V) compared with AVFR (T-T) causes the experimental results to be predicted more accurately.
3- The value and sign of the Lode parameter along with the value of plastic modulus in isotropic hardening problems has a direct effect on difference between the proposed NAVFR and AVFR.
4- Combination of loading (tension-shear) can cause differences between the presented NAFVR and corresponding AFVR such that for $\Gamma \longrightarrow \pm 1$ these differences increase and for $\Gamma \longrightarrow 0$ they decrease.

6. REFERENCES

1. Stoughton, T. B. and Yoon, J.-W., "A pressure-sensitive yield criterion under a non-associated flow rule for sheet metal forming", ***International Journal of Plasticity***, Vol. 20, No. 4, (2004), 705-731.
2. Nukala, P. K. V., "A return mapping algorithm for cyclic viscoplastic constitutive models", ***Computer Methods in Applied Mechanics and Engineering***, Vol. 195, No. 1, (2006), 148-178.
3. Ohno, N. and Wang, J., "Kinematic hardening rules for", ***European Journal of Mechanics, A/Solids***, Vol. 13, No. 4, (1994), 519-531.
4. Liang, L., Liu, Y. and Xu, B., "Design sensitivity analysis for parameters affecting geometry, elastic–viscoplastic material constant and boundary condition by consistent tangent operator-based boundary element method", ***International Journal of Solids and Structures***, Vol. 44, No. 7, (2007), 2571-2592.
5. Cvitanić, V., Vlak, F. and Lozina, Ž., "A finite element formulation based on non-associated plasticity for sheet metal forming", ***International Journal of Plasticity***, Vol. 24, No. 4, (2008), 646-687.
6. Stoughton, T. B. and Yoon, J. W., "Anisotropic hardening and non-associated flow in proportional loading of sheet metals", ***International Journal of Plasticity***, Vol. 25, No. 9, (2009), 1777-1817.
7. Gao, X., Zhang, T., Hayden, M. and Roe, C., "Effects of the stress state on plasticity and ductile failure of an aluminum 5083 alloy", ***International Journal of Plasticity***, Vol. 25, No. 12, (2009), 2366-2382.
8. Mohr, D., Dunand, M. and Kim, K.-H., "Evaluation of associated and non-associated quadratic plasticity models for

advanced high strength steel sheets under multi-axial loading", ***International Journal of Plasticity***, Vol. 26, No. 7, (2010), 939-956.

9. Romano, G., Barretta, R. and Diaco, M., "Algorithmic tangent stiffness in elastoplasticity and elastoviscoplasticity: A geometric insight", ***Mechanics Research Communications***, Vol. 37, No. 3, (2010), 289-292.
10. Taherizadeh, A., Green, D. E. and Yoon, J. W., "Evaluation of advanced anisotropic models with mixed hardening for general associated and non-associated flow metal plasticity", ***International Journal of Plasticity***, Vol. 27, No. 11, (2011), 1781-1802.
11. Gao, X., Zhang, T., Zhou, J., Graham, S. M., Hayden, M., and Roe, C., "On stress-state dependent plasticity modeling: Significance of the hydrostatic stress, the third invariant of stress deviator and the non-associated flow rule", ***International Journal of Plasticity***, Vol. 27, No. 2, (2011), 217-231.
12. Voyiadjis, G. Z., Shojaei, A. and Li, G., "A generalized coupled viscoplastic–viscodamage–viscohealing theory for glassy polymers", ***International Journal of Plasticity***, Vol. 28, No. 1, (2012), 21-45.
13. Voyiadjis, G. Z. and Abu Al-Rub, R. K., "Thermodynamic based model for the evolution equation of the backstress in cyclic plasticity", ***International Journal of Plasticity***, Vol. 19, No. 12, (2003), 2121-2147.
14. Berga, A., "Mathematical and numerical modeling of the non-associated plasticity of soils—part 1: The boundary value problem", ***International Journal of Non-Linear Mechanics***, Vol. 47, No. 1, (2012), 26-35.
15. Moayyedian, F. and Kadkhodayan, M., "A general solution in rate-dependant plasticity", ***International Journal of Engineering***, Vol. 26, No., (2013), 391-400.
16. Hinton, E. and Owen, D., "Finite elements in plasticity: Theory and practice", ***Pineridge, Swansea, Wales***, Vol., No., (1980).
17. de Souza Neto, E. A., Peric, D. and Owen, D. R. J., "Computational methods for plasticity: Theory and applications", John Wiley & Sons, (2011).
18. Simof, J. and Hughes, T., "Computational inelasticity", (2008).
19. Zienkiewicz, O. C. and Taylor, R. L., "The finite element method for solid and structural mechanics", Butterworth-Heinemann, (2005).
20. Crisfield, M., Remmers, J. and Verhoosel, C., "Nonlinear finite element analysis of solids and structures", John Wiley & Sons, (2012).
21. Hill, R., "The mathematical theory of plasticity", Oxford university press, Vol. 11, (1998).
22. Chakrabarty, J., "Theory of plasticity", Butterworth-Heinemann, (2006).
23. Chen, W.-F. and Zhang, H., "Structural plasticity: Theory, problems and cae software", Springer-Verlag New York, Inc., (1990).
24. Huang, S., "Continuum theory of plasticity", Wiley. com, (1995).
25. Marcal, P., "A note on the elastic-plastic thick cylinder with internal pressure in the open and closed-end condition", ***International Journal of Mechanical Sciences***, Vol. 7, No. 12, (1965), 841-845.

A Study on Combination of von Mises and Tresca Yield Loci in Non-associated Viscoplasticity

F. Moayyedian, M. Kadkhodayan

Department of Mechanical Engineering, Ferdowsi University of Mashhad, Mashhad, Iran

PAPER INFO

Paper history:
Received 08 April 2013
Received in revised form 10 July 2013
Accepted 22 August 2013

Keywords:
Viscoplastic
Thick Walled Cylinder
Time Stepping Scheme
Internally Pressurized

چکیده

در این پژوهش قانون جریان ویسکوپلاستیسیته ناوابسته (NAVFR) با ترکیب سطوح تسلیم ون مایزز و ترسکا به جای توابع تسلیم و پتانسیل پلاستیک و برعکس ارائه شده است. به کمک روش مرحله ای زمانی کاملا غیرصریح و همچنین بررسی در مورد مطالعات انجام شده روی توابع پتانسیل پلاستیک ارائه شده توسط سایر مولفین و همچنین نتایج آزمایشگاهی نشان داده خواهد شد که قانون جریان ویسکوپلاستیسیته ناوابسته ارائه شده از قانون جریان وابسته (AVFR) مرسوم نظیر خود نتایج آزمایشگاهی را دقیق‌تر پیش بینی می‌نماید.

doi: *10.5829/idosi.ije.2014.27.03c.12*